



Mechanical behavior and fracture characterization of a monocrystalline Cu–Al–Ni subjected to thermal cycling treatments under load

L.A. Matlakhova^{a,*}, E.C. Pereira^a, A.N. Matlakhov^a, S.N. Monteiro^a, R. Toledo^b

^aState University of the Northern Rio de Janeiro, UENF, Advanced Materials Laboratory, LAMAV, Av. Alberto Lamego, 2000, Parque Califórnia, Campos dos Goytacazes, RJ, CEP 28013-602*, Brazil

^bState University of the Northern Rio de Janeiro, UENF, Laboratory of Physical Science, LCFIS, Av. Alberto Lamego, 2000, Parque Califórnia, Campos dos Goytacazes, RJ, CEP 28013-602*, Brazil

ARTICLE DATA

Article history:

Received 21 January 2008

Accepted 1 March 2008

Keywords:

Monocrystalline Cu–Al–Ni alloy

Reversible martensitic transformation

Thermal cycling treatment

Structural characterization

Mechanical properties

ABSTRACT

The mechanical behavior and fracture characteristics resulting from thermal cycling treatments under different applied loads were investigated in a monocrystalline Cu–13.5 wt.%Al–4.0 wt.%Ni alloy. The treatments consisted of 300 cycles in the temperature interval between 0 °C (close to M_f) and 100 °C (above A_f), under applied load conditions of 0.2 and 0.5 kg corresponding, respectively, to stresses of 11×10^{-2} and 28×10^{-2} MPa. Following each treatment, the specimens were tested in compression until fracture at room temperature. In addition to the compression results, the mechanical behavior was also evaluated by microhardness tests. Structural changes related to phase transformations were characterized by X-ray diffraction and the fracture characteristics were analyzed by scanning electron microscopy. It was found that the thermal cycling treatments promote significant changes in the structure due to a reversible martensitic transformation. An increase in the applied load results in a decrease in both the pseudo-yield and the total strain. It also results in a lower fracture resistance owing to additional deformation accumulated during the cycling treatment, which provokes the reversible martensitic transformation.

© 2008 Elsevier Inc. All rights reserved.

1. Introduction

A reversible (thermoelastic) martensitic transformation (RMT), which was later found to be associated with the shape memory effect [1], was discovered in Cu-based alloys by Kurdjumov and Khandros [2,3]. This finding was soon followed by the first observation of superelastic behavior in Au–Cd by Chang and Read [4] and “rubbery” behavior in In–Tl by Basinski and Christian [5], both being non-elastic effects in alloys. Long after these works, the phenomenon of the shape memory effect (SME) was discovered in TiNi alloys by Buehler et al. [1] and innumerable projects regarding potential SME applications

impelled further investigations. It was subsequently determined that the SME and other non-elastic effects (NEE) are correlated with RMT [6–9]. Since then, the alloys exhibiting RMT, either as SME or other NEE, have been the subject of extensive investigations [6–13]. Many of these alloys are now being used in a variety of practical systems related to the fields of engineering and medicine [14–20].

Among these alloys, the TiNi based alloys are considered the most promising for technological applications owing to their superior SME parameters, associated with good mechanical properties and excellent resistance to corrosion [8,11,15,16,21–23]. TiNi based alloys are, however, relatively

* Corresponding author. Tel.: +55 22 2726 1525 29; fax: +55 22 2726 1525 24.

E-mail addresses: lioudmila@uenf.br, lioudmila@globo.com (L.A. Matlakhova), elainecp@uenf.br (E.C. Pereira), anatoli@uenf.br (A.N. Matlakhov), sergio.neves@ig.com.br (S.N. Monteiro), toledo@uenf.br (R. Toledo).

expensive and hence other SME alloys have also been proposed. Less expensive Cu-based SME alloys present additional advantages in terms of superior electrical and thermal conductivities [24–26]. Moreover, their deformability, which is an important property for wire fabrication, is better than that of TiNi SME alloys [26]. In the case of polycrystalline Cu–Al–Ni, the alloy's low deformability is, however, an exception. These alloys are susceptible to intergranular cracking, which limits the scope of many potential applications. It was found [24] that the reason for Cu–Al–Ni intergranular cracking is the formation of stress-induced martensite along grain boundaries upon quenching.

Polycrystalline SME alloys, in general, are not as effective as single crystals in terms of SME parameters. The recoverable strains in the former are considerably reduced since an applied stress generates strains that differ from grain to grain and on average, for the bulk material, are close to zero. For this reason, and the above-mentioned occurrence of intergranular cracking, polycrystalline Cu–Al–Ni SME alloys present inherent limitations that limit their mechanical response for practical SME purposes [17,26].

Special attention is currently being paid to monocrystalline Cu–Al–Ni alloys owing to their desirable SME parameters, in association with a tendency not to accumulate non-reversible plastic deformation [17,27–29]. In comparison with similar polycrystalline alloys, monocrystalline Cu–Al–Ni presents higher pseudo-elastic deformation, up to 12%, and SME back stress above 600 MPa, as well as a low level of residual deformation [11,30].

One of the limitations for the practical application of an SME alloy is the alteration in behavior which develops after multiple thermal cycles. Cycling within the temperature interval of martensite transformation is known to cause changes in the substructure and phase composition as well as a consequent modification in the physical and mechanical properties of the alloys [11,27,28]. In fact, each thermal cycle may produce additional dislocations that, in turn, may interfere with the martensitic transformation. These dislocations might be responsible for shifts in the values of the characteristic temperatures associated with the RMT [31]. In the previous work cited above, however, the effect of a superimposed stress during a thermal cycling treatment (TCT) had not been evaluated.

The objective of this work was therefore to investigate the changes in the structure, mechanical behavior and the fracture surface morphology that occurred as a result of stress-assisted TCT performed under two different levels of loading and compression deformation up to cracking, in a monocrystalline copper-based alloy with 13.5 wt.% Al and 4.0 wt.% Ni.

2. Materials and Methods

The monocrystalline Cu-13.5Al-4Ni alloy used in this work was fabricated in the form of a cylindrical bar of 5 mm in diameter at the “Memory Crystals Group” of the Technical University of Saint Petersburg, Russia [32]. The phase composition of the alloy was determined by X-ray diffraction (XRD) in DRON-3M and URD-65 diffractometers using Cu-K α and Co-K α radiations, respectively, for 2θ angles from 25 to 75° at

scanning steps of 0.03°/3 s and 0.05°/3 s, both operating at ambient temperature.

Specimens in the form of discs, 5 mm in thickness, were sectioned perpendicular to the axis of the bar using a MINITON cutter. The flat surfaces of each specimen were polished with 0.1 μm alumina paste. No chemical attack was used since the final fracture, rather than the developed microstructure, was of interest in the present work. The specimens were then submitted to 300 thermal cycles under load (300 TCTs) consisting of heating above A_f , up to 100 °C, and cooling down to 0 °C, near the M_f . After the 300 cycles the process was terminated with a last partial cycle of heating from 0 °C to room temperature (RT). The 300 TCTs were performed under two different applied loads, of 0.2 and 0.5 kg, corresponding to stresses of 11×10^{-2} and 28×10^{-2} MPa, respectively. The load was applied in a device specially developed for this purpose. The reason for these two levels of applied load will be further justified.

Compression tests after the 300 TCTs were carried out at RT until fracture, in a model 5582 Instron machine operating with a crosshead speed of 0.1 mm/min. Vickers microhardness measurements of the specimens were performed in a Neophot-32 optical microscope coupled with a MHP-100 device. The fracture surfaces of these specimens were analyzed by scanning electron microscopy in a model DSM-962 Zeiss microscope. Scanning electron microscopy images were obtained with secondary electrons accelerated at 15 kV.

3. Results and Discussion

The results obtained after 300 TCTs under load were compared with corresponding results for the Cu-13.5Al-4Ni alloy in its initial state, as a quenched structure, without any cycling or applied load.

Fig. 1 presents the XRD patterns for the alloy in its initial state (a) and after the 300 TCT under the two different applied loads of 0.2 (b) and 0.5 kg (c). In its initial state, Fig. 1(a), the Cu-13.5Al-4Ni alloy displays three metastable phases: the type DO₃ high temperature β_1 ordered phase [33a], the type Cu₃Ti ordered martensitic γ'_1 phase [33b] and the rhombohedral ordered Al₇Cu₄Ni phase [33c,34], which will here be referred to as the R phase. The high temperature β_1 is represented in Fig. 1 (a) by an intensive (331) β_1 peak while the martensitic γ'_1 exhibited two (022) γ'_1 and (111) γ'_1 peaks with relatively lower intensity. Two additional (107)_R and (2014)_R peaks, in Fig. 1(a), could be associated with the rhombohedral R phase. Another (0015)_R peak of the R phase is practically coincident with the (111) γ'_1 peak of the martensitic γ'_1 [33b–34]. In previous work [28] on the initial state of a similar alloy the presence of the R phase could not be revealed by optical microscopy. As a possible explanation for this, it was suggested that the R phase could be interpreted as being coherent with other existing phases and, therefore, regarded as an intermediate phase that is stabilized at RT.

After the 300 TCTs under an applied load of 0.2 kg, the results shown in Fig. 1(b) exhibit peaks corresponding to the β_1 and the martensitic γ'_1 are also still observed. Moreover, the coherent γ'_1 R peak found in the initial state, Fig. 1(a), as well

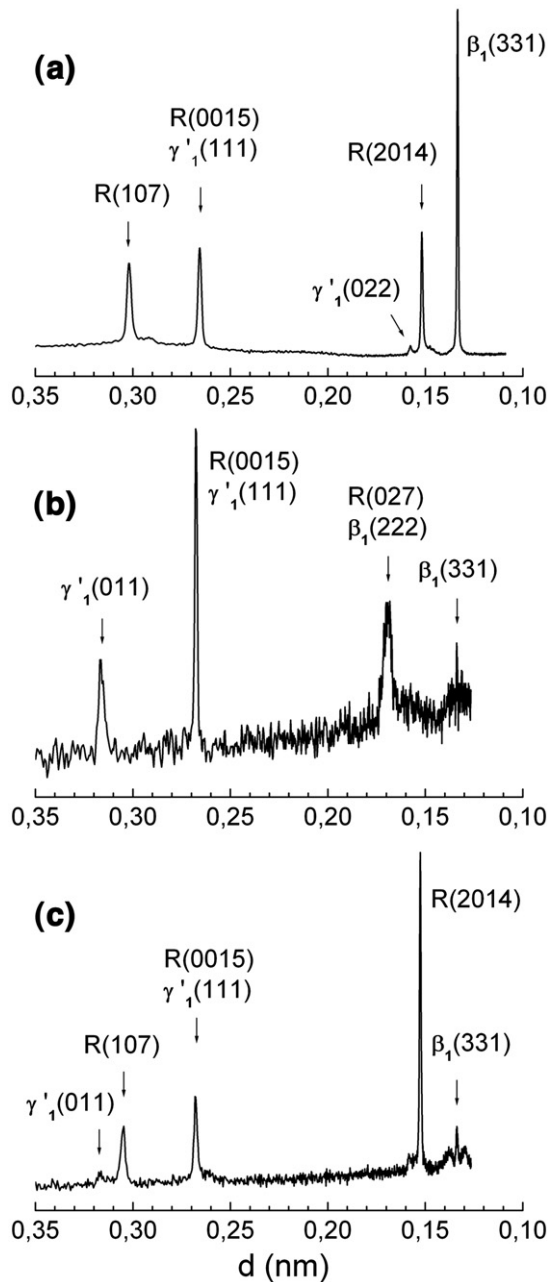


Fig. 1—XRD patterns of the alloy Cu-13.5Al-4Ni in its initial state (a) and after the 300 TCT under applied loads of 0.2 kg (b) and 0.5 kg (c).

as another coherent peak composed of $(222)_{\beta_1}$ and $(027)_R$ are also observed. The relatively high intensity peaks of the coherent phases can be regarded as an indication of greater stability of the intermediate state after treatment.

The alloy submitted to 300 TCTs under an applied load of 0.5 kg, Fig. 1(c), displays an intense $(2014)_R$ and a relatively moderate intensity $(107)_R$ peaks corresponding to the R phase. The participation of the martensitic γ'_1 can now be detected by the coherent, moderate intensity, $(111)_{\gamma'_1}[(0015)_R]$ peak. Here it should be noted that the $(331)_{\beta_1}$ peak of the β_1 phase is decreased in intensity, Fig. 1(c), compared to that of the initial state depicted in Fig. 1(a).

Fig. 2 presents the XRD patterns of the alloy after compression until fracture for the same conditions: (a) initial state, (b) 300 TCTs under 0.2 kg and, (c) 300 TCTs under 0.5 kg load. The XRD analysis of the alloy in its initial state after fracture, Fig. 2(a), shows an intense coherent $(111)_{\gamma'_1}[(0015)_R]$ peak for the martensitic γ'_1 and R phases. Another $(331)_{\beta_1}$ peak with lower intensity is related to the β_1 phase.

The sample subjected to 300 TCTs under 0.2 kg followed by compression until fracture, Fig. 2(b), exhibits the same peaks as in Fig. 2(a) in addition to a very low intensity $(2014)_R$ peak associated with the R phase. The sample subjected to 300 TCTs under 0.5 kg after compression until fracture, Fig. 2(c), presents an XRD pattern indicating a greater participation of

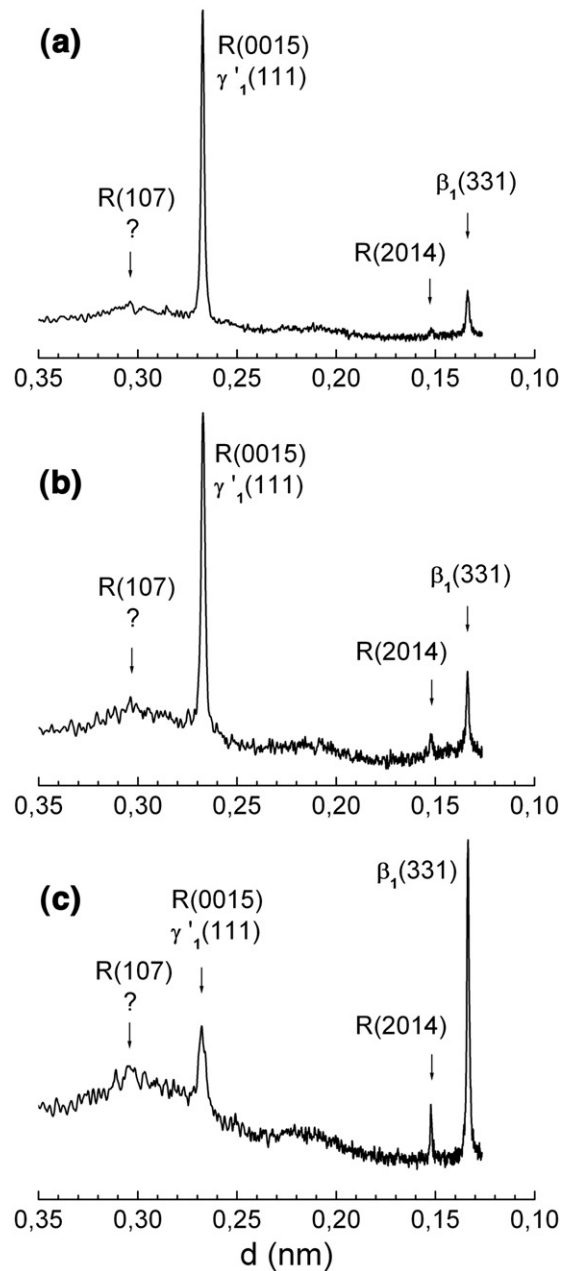


Fig. 2—XRD patterns of the alloy Cu-13.5Al-4Ni after compression until fracture for the: (a) initial state and after 300 TCT under (b) 0.2 kg and (c) 0.5 kg.

the β_1 phase, as represented by its $(331)_{\beta_1}$ peak. Moreover, both the R phase, detected by its own $(2014)_R$ and $(107)_R$ peaks, as well as the martensitic γ'_1 phase, by its coherent moderate intensity $(111)_{\gamma'_1}|| (0015)_R$ peaks, are also revealed in Fig. 2(c).

The XRD patterns in Figs. 1 and 2 indicate that an increase in applied load during the 300 TCTs favors a coherent interface between the R phase and the γ'_1 phase. At the end of the 300 TCTs, during heating from 0 °C up to room temperature, the applied load promotes the reverse martensitic transformation $\gamma'_1 \rightarrow R \rightarrow \beta_1$ as noted in TiNi alloys [35–38]. However, by unloading the specimen to perform the XRD analysis, the structure may suffer a relaxation process followed by a transformation in the opposite direction, $\beta_1 \rightarrow R \rightarrow \gamma'_1$. This can be explained by the fact that the active stress is associated with an unstable thermodynamic state. It is proposed that structural imperfections accumulated during the 300 TCTs under load, would retard all RMT reactions, not only retaining but also enhancing both the R and the martensitic γ'_1 metastable phases.

Specimens that were subjected to the 300 TCTs under the smaller load of 0.2 kg followed by compression until fracture, Fig. 2(b), showed a greater incidence of the transient R phase coherent to the γ'_1 phase. By contrast, the accumulation of more plastic deformation in the fracture of specimens submitted to 300 TCTs under the larger applied load of 0.5 kg, resulted in a pronounced incidence of the stress-induced β_1 phase, as depicted in Fig. 2(c), due to the RMT $\gamma'_1 \rightarrow R \rightarrow \beta_1$ reaction.

The stress–strain curves in Fig. 3 show the mechanical behavior of the Cu-13.5Al-4Ni alloy in its initial state (curve 1) as well as after the 300 TCTs under applied loads of 0.2 kg (curve 2) and 0.5 kg (curve 3). It should be noted in this figure that all curves display, approximately, the same general behavior. A very small initial elastic part of each curve is followed by a relatively extensive “pseudo-yield” plateau, which is typical of alloys presenting non-elastic effects [11]. Subsequently, another steeper elastic section continues up to fracture. The specific parameters related to each of these curves, however, show perceptible differences.

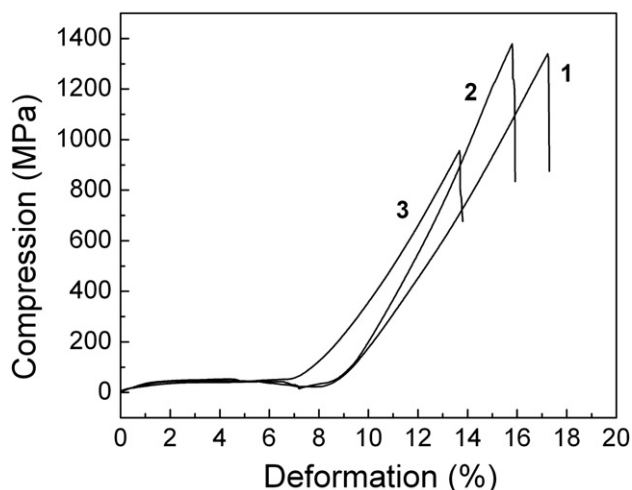


Fig. 3 – Stress–Strain curves up to fracture for the Cu-13.5Al-4Ni alloy: (1) initial state and after 300 TCT under: (2) 0.2 kg, (3) 0.5 kg of applied load.

Table 1 – Vickers microhardness (HV) of the Cu-13.5Al-4.0Ni alloy in initial state and after the 300 TCT under applied load of 0.2 kg and 0.5 kg

Alloy condition	HV(kgf/mm ²)
Initial state	300.5 ± 20.4
300 TCT under 0.2 kg	318.4 ± 24.5
300 TCT under 0.5 kg	342.8 ± 47.2

In its initial state, curve 1, the alloy displays around 8% strain for the “pseudo-yield” deformation at a 60–65 MPa level of stress. In this interval, an accumulation of reversible deformation occurs in relation to the SME and is accompanied by $\gamma'_1 \rightarrow \beta_1$ RMT and reorientation of the initial structure. For strains beyond the “pseudo-yield”, i.e. 8%, linear elastic behavior occurs up to rupture, which takes place at an ultimate stress of 1350 MPa for a total strain of 17.2%. The high strength attained by the alloy can be attributed to a number of dislocations introduced during the “pseudo-yield” deformation [31]. Similar results were obtained in previous research [30] where Cu–Al–Ni monocrystalline alloys, with compositions comparable to that of the alloy in the present work, were investigated.

In Fig. 3 it can also be seen that the alloy submitted to the 300 TCTs under an applied load of 0.2 kg, curve 2, in compression exhibits a “pseudo-yield” strain, of 8%, a rupture stress of 1370 MPa, and a total strain of 15.8%, which are very close to the values of curve 1, corresponding to the initial state. Here it is worth noticing that the XRD patterns, Fig. 2(a, b) also display an analogous situation with a greater incidence of the transient R phase coherent to the γ'_1 phase.

In Fig. 3 the alloy submitted to the 300 TCTs under an applied load of 0.5 kg, curve 3, shows significant differences associated with lower values of the “pseudo-yield” strain of 6.5%, rupture stress of 956 MPa, and total strain of 13.5%, as compared to curves 1 and 2. This corresponds to reductions of 41% and 30% in the maximum stress and total strain, respectively, as compared with the initial state. Apparently, under this load of 0.5 kg, the number of accumulated dislocations [31] is sufficient to interfere with the RMT causing a decrease in the SME parameters.

Here it is important to explain the reason for the choice of both levels of load in the present work. The applied load of 0.2 kg was found to be the maximum for which no apparent change was caused to the mechanical behavior of the alloy by thermal cycling. On the other hand, the applied load of 0.5 kg was the minimum for which clear decreases were obtained in the mechanical parameters.

Microhardness is another mechanical property which adds to the understanding of the behavior of the monocrystalline Cu-13.5Al-4Ni alloy. The Vickers microhardness (HV) of the alloy in its initial state and after the 300 TCTs under the two applied loads of 0.2 and 0.5 kg are presented in Table 1.

In this table one should note a tendency of increasing HV with thermal cycling as compared to the initial state. Moreover, the larger applied load of 0.5 kg, also results in higher HV. A simple explanation for this behavior can be given in terms of the possible accumulation of dislocations during thermal cycling [31]. The greater number of dislocations associated

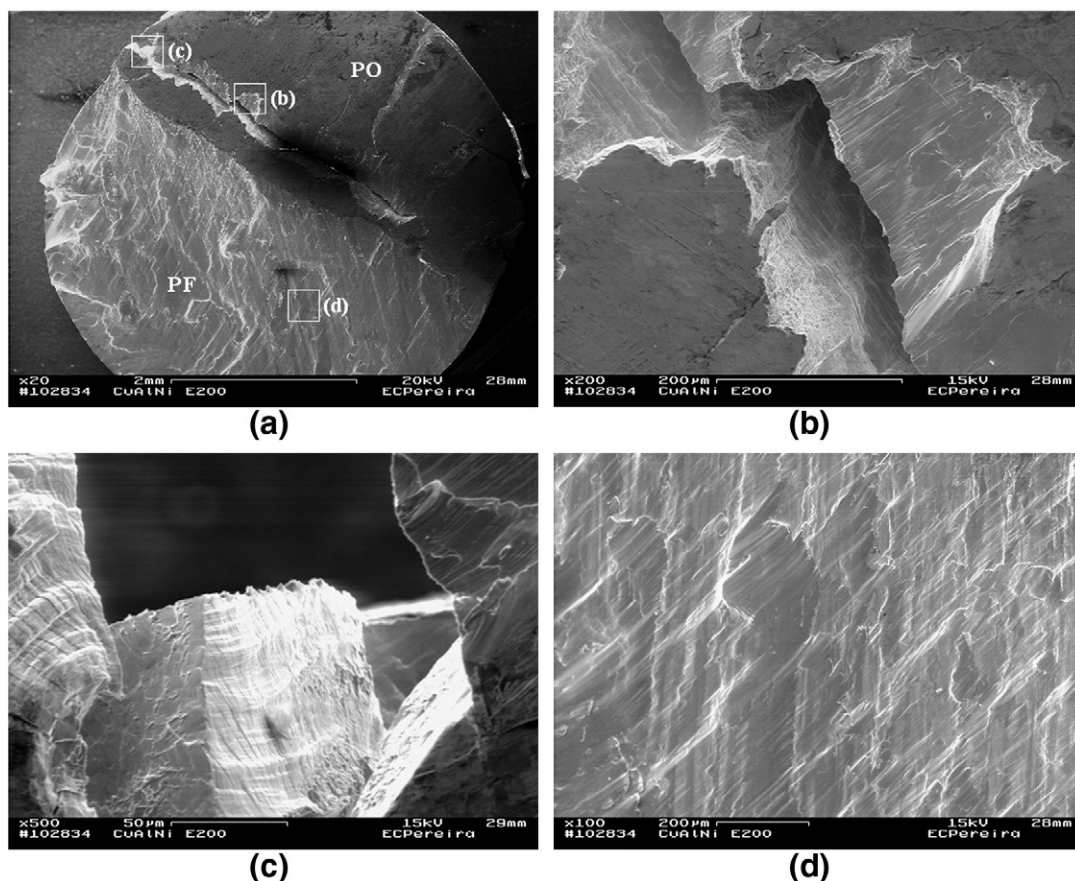


Fig. 4—Scanning electron microscopy images of the fracture surface of the Cu-13.5Al-4.0Ni alloy in its initial state.

with the 300 TCTs under 0.5 kg also explains the HV increase in comparison with the 300 TCTs under 0.2 kg shown in Table 1. Here it is also interesting to note that the 300 TCTs under 0.5 kg condition, corresponding to the higher HV, presents the larger band of uncertainty (statistical error) associated with the standard deviation. This can be attributed to the non-uniform accumulation of defects due to the nature of the martensitic transformation, as well as to the correlation of the applied stress with preferential planes and directions active in the martensitic transformations, which results in regions with different dislocation densities.

The fracture characteristics of the monocrystalline Cu-13.5Al-4Ni alloy, corresponding to the three investigated conditions, are presented in Figs. 4–6. A common aspect observed in all conditions is the brittle nature of the fracture, which was also reported in previous research [30] investigating comparable Cu–Al–Ni alloys. As a general observation, it is important to bear in mind that a crack always initiates at a point on the specimen's flat surfaces that are in contact with the compressing plates of the Instron machine. Rupture then propagates following single or different planes, inclined at 45° with respect to the direction of uniaxial compression.

During fracture in compression of the specimen corresponding to the initial state, Fig. 4, a crack propagated in a single plane almost through to the middle of the cross section as shown at low magnification in Fig. 4(a). In this figure, the unbroken part of the original specimen's flat surface, which

was in contact with the plate, is labeled as PO, while the plane of fracture as PF. In addition to the main crack that initiated the fracture, another relatively large secondary crack can be seen in the original flat surface. This secondary crack was already propagating, Fig. 4(b), when the main crack broke the specimen. A detached polyhedral-shaped block can be seen, Fig. 4(c), at the extremity of the secondary crack. This block is apparently associated with a martensite packet, which was previously observed by optical microscopy at the periphery of similar alloys [28]. With higher magnification, Fig. 4(d), the plane of fracture displays “river patterns” typical of the cleavage-like rupture associated with the propagation of the main crack.

The fracture appearance of the alloy subjected to 300 TCTs under 0.2 kg, and then submitted to compression until rupture, is shown in Fig. 5. At low magnification, Fig. 5(a), one can see that the fracture occurred in two planes, PF1 and PF2. Similar to Fig. 4(a), for the initial state, part of the original specimen's flat surface (PO) was left intact. By contrast, the fracture surface presents differences with respect to those of the initial state. The rupture process in this case is associated more with slip lines, Fig. 5(b), rather than cleavage-like marks. This is apparently a consequence of the number of dislocations introduced by the thermal cycles [31]. A small polyhedral block was also observed, Fig. 5(c, d), at the border between two fracture surfaces. The same interpretation of a martensite packet is suggested for this block [28]. In addition,

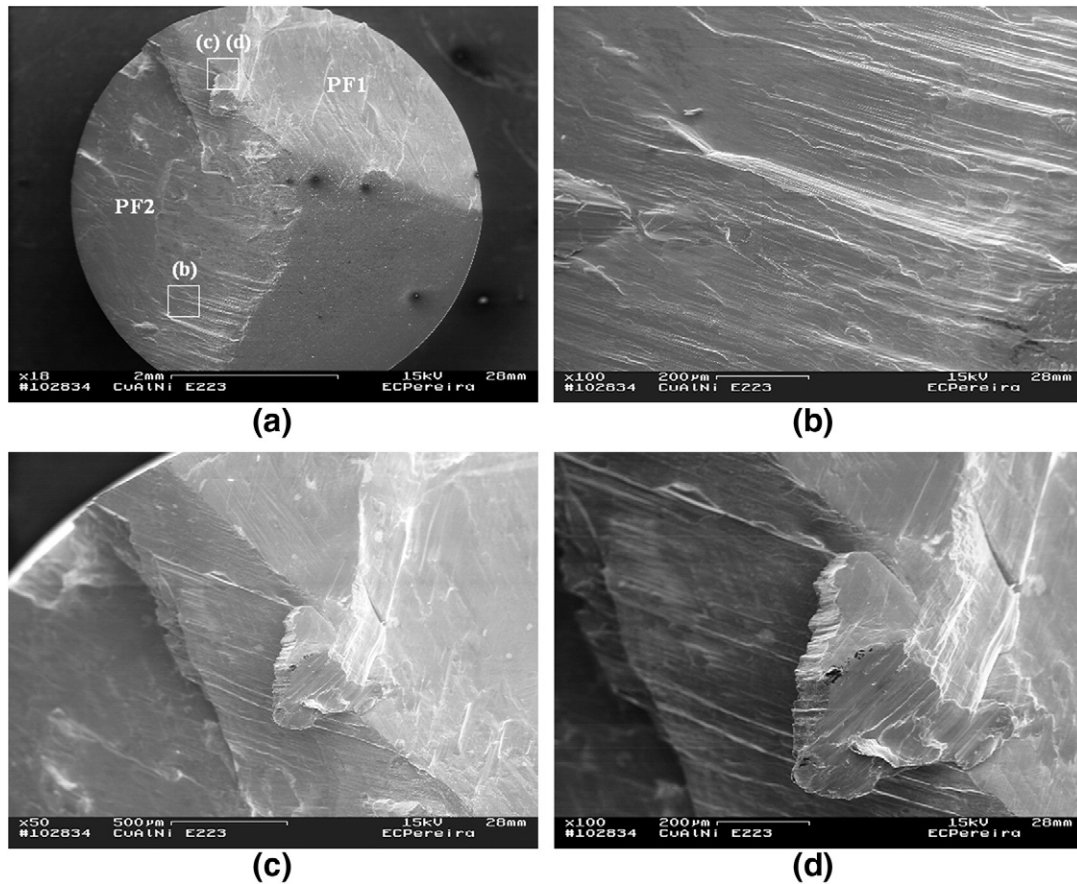


Fig. 5 – Scanning electron microscopy images of the fracture surface of the Cu-13.5Al-4.0Ni alloy after 300 TCT under an applied load of 0.2 kg.

the location of this block indicates that it may serve as an initiation point for crack nucleation. If this is the case, the change in martensite orientation within the structure of a monocrystalline alloy can play a relevant role in the fracture behavior.

The fracture in compression of the alloy after the 300 TCTs under 0.5 kg is presented in Fig. 6. At low magnification, Fig. 6 (a), two planes of fracture (PF1 and PF2) can be observed in a similar manner as the sample subjected to 300 TCTs under 0.2 kg previously shown in Fig. 5(a). However, contrary to the initial state, Fig. 4(a), and the sample subjected to 300 TCTs under 0.2 kg, Fig. 5(a), no part of the original specimen's flat surface remains. With higher magnification, Fig. 6(b), the fracture surface could be associated with slip lines and cross-slip from different deformation systems. The protruding edges at the right side of Fig. 6(b) indicate a slippage process along preferential planes caused by dislocation movement. Moreover, other areas of the fracture surface, Fig. 6(c), present a rough aspect typical of intense plastic deformation. This is in agreement with the influence of the 0.5 kg level of applied load, on the mechanical behavior of the alloy, as mentioned before. A small polyhedral block can also be seen in Fig. 6(d) at the intersection of two fracture surfaces. This martensite packet could have been the site of crack nucleation, as in the initial state, Fig. 4(c), and the sample subjected to 300 TCTs under 0.2 kg, Fig. 5(c, d).

4. Conclusions

The thermal cycling treatments under different loads within the temperature interval of the reversible martensitic transformation of a Cu-13.5Al-4Ni alloy, revealed that the metastable β_1 , γ'_1 and R phases found in the initial quenched state were not significantly affected by the cycling treatments, except for a decrease in the incidence of β_1 . After compressions until fracture, these same phases were observed and the peak intensities indicate that the applied load favors the existence of the R phase coherent to the γ'_1 phase.

The compression behavior determined by stress-strain curves is very similar for the alloy in its initial state and after the cycling treatment under the smaller load of 0.2 kg. However, the cycling treatment under 0.5 kg significantly decreases the pseudo-yield strain and the rupture stress, as an apparent consequence of dislocation accumulation.

The increase in microhardness, from the initial state, associated with the cycling treatments can also be attributed to the accumulation of crystalline defects.

In fracture under compression, a cleavage pattern is observed for the initial state, corresponding to the brittle nature of the rupture mode. By contrast, for the alloy thermally treated under load, the fracture surface is associated with slip lines indicating the participation of

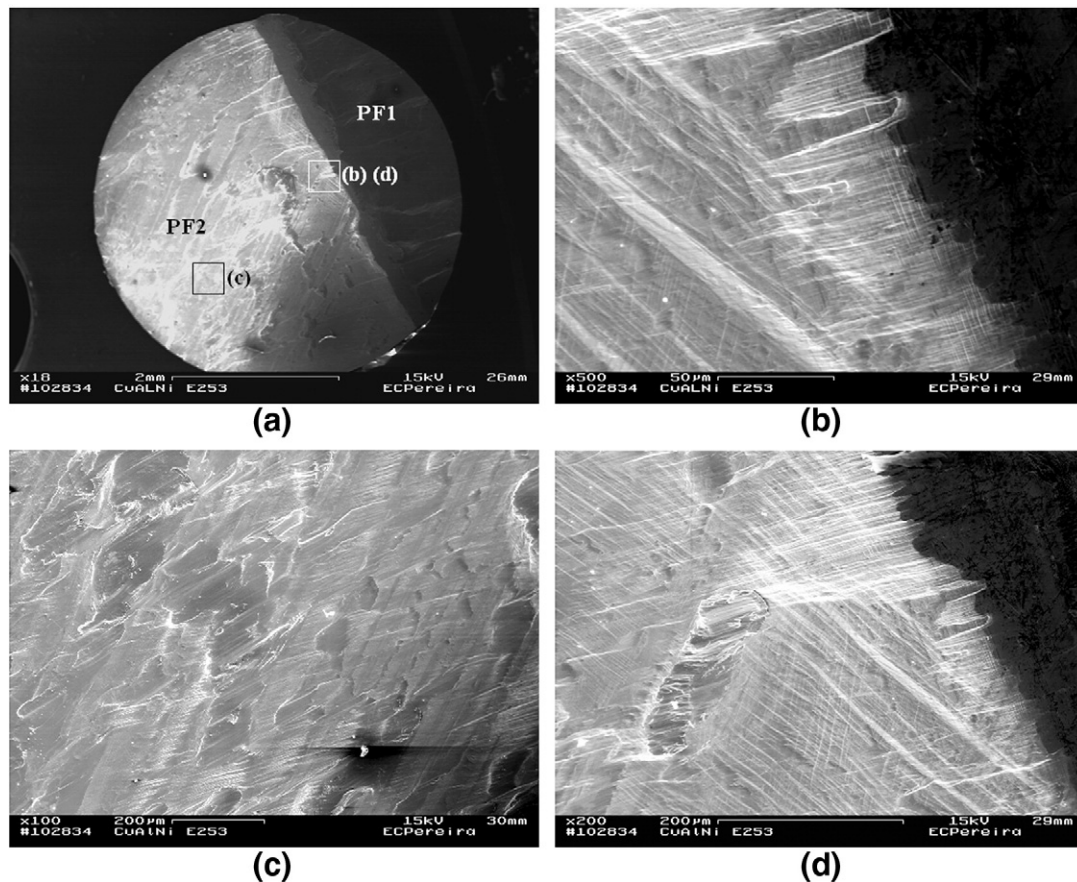


Fig. 6 – Scanning electron microscopy images of the fracture surface of the Cu-13.5Al-4.0Ni alloy after 300 TCT under an applied load of 0.5 kg.

dislocations in the process of rupture. In all cases, the presence of martensite packets in the form of polyhedral blocks serves as a preferential site for crack nucleation.

Acknowledgements

The authors thank the Brazilian agencies CNPq, CAPES and FAPERJ for supporting this work. We also acknowledge the collaboration of professor Eduardo Atem de Carvalho (UENF) for the deformation tests.

REFERENCES

- [1] Buehler WJ, Gilfrich JV, Wiley RC. Effect of low-temperature phase changes on the mechanical properties of alloys near composition TiNi. *J Appl Phys* 1963;34:1475–7.
- [2] Kurdymov GV. Diffusionless (martensitic) transformations in alloys. *J Techn Phys* 1948;18:999–1025 (in Russian).
- [3] Kurdymov GV, Khandros LG. About the thermoelastic equilibrium in martensite transformations. *Dokl Akad Nauk SSSR* 1949;2:214–21 (in Russian).
- [4] Chang LC, Read TA. Plastic deformation and diffusionless phase changes in metals. The gold–cadmium beta phase. *Trans AIME* 1951;189–1:47–52.
- [5] Basinski ZS, Christian JW. Crystallography of deformation by twin boundary movement in indium–thallium alloys. *Acta Metall* 1954;2:101–16.
- [6] Perkins J. Shape memory effects in alloys. *Proc Int Conf on Shape Memory Effects and Applications*. Toronto–Ontário, Canada; 1975. 470p.
- [7] Otsuka K, Shimizu K. Memory effect and thermoelastic martensite transformation in Cu–Al–Ni alloy. *Scripta Metallurgica* 1970;4:469–72.
- [8] Otsuka K. Origin of memory effect in Cu–Al–Ni alloy. *Jpn J Appl Phys* 1971;10:571–9.
- [9] Delaey L, Deruyttere A, Aernoudt N, Roos JR. Shape memory effect, super-elasticity and damping in Cu–Zn–Al Alloys. *INGRA Res Proj* 1978;238:91.
- [10] Miyazaki S, Kawai T, Otsuka K. Martensitic transformations. *Proc Int Conf on ICOMAT*. Leuven, Belgium, vol. 4; 1982. 813p.
- [11] Otsuka K, Wayman CM, editors. *Shape memory materials*. Cambridge: University Press; 1999.
- [12] Huang W, Liu QY, Ong LF. Assembly of hard disk drive using shape memory alloys. *Proc Asia-Pacific Magnetic Recording Conference*. Singapore; August 27–29 2002.
- [13] Sehitoglu H, Hamilton RF, Efstathiou C, Chumlyakoy YI, Maier HJ. Mechanical hysteresis in single crystal shape memory alloys. *Proc Int Conf on shape memory and superelastic technologies*. California, USA; May 7–11 2006.
- [14] Nikolaev V, Pulnev S, Priadko A, Vahhi I, Bhattacharyya A. Actuators and drives based on CuAlNi shape memory single crystals. *Proc Int. Conf on shape memory and superelastic technologies*. California, USA; May 7–11 2006.

- [15] Duerig T, Pelton A, Stöckel D. An overview of nitinol medical applications. *Mater Sci Eng A* 1999;273–275:149–60.
- [16] Auricchio F, Petrini L, Pietrabissa R, Sacco E. Shape-memory alloys in orthodontics: mechanical, experimental, modeling and clinical considerations. Proc workshop on shape memory alloy materials. Experimental investigation, modeling, metallurgy, applications Warsaw, Poland; September 2001.
- [17] Martynov V, Bokaie MD, Johnson AD, Gray GR. Superelastic and shape memory single crystal CuAlNi: fabrication and applications. Proc Int Conf on shape memory and superelastic technologies. California, USA; May 7–11 2006.
- [18] Unterweger E, Lojen G, Kneissl A, Anzel I, Kosec B, Bizjak M. Characterisation of Cu–Al–Ni melt-spun ribbons after different thermal and mechanical treatments. Proc Int Conf on shape memory and superelastic technologies. Editor Matthias Mertmann. Baden-Baden, Germany; October 3–7 2004.
- [19] Lexcelent C. The rational use of shape memory alloys as actuators or dampers. Proc Int Conf on shape memory and superelastic technologies. California, USA; May 7–11 2006.
- [20] Motahari SA, Ghassemieh M. Multilinear one-dimensional shape memory material model for use in structural engineering applications. *Eng Struct* 2007;6:904–13.
- [21] Duerig TW, Pelton AR. Titanium alloys. In: Boyer R, Welsch G, Collings EW, editors. *Materials properties handbook*. USA: ASM International; 1994. p. 1035–48.
- [22] Otsuka K, Ren X. Martensitic transformations in nonferrous shape memory alloys. *Mater Sci Eng A* 1999;273–275:89–105.
- [23] Otsuka K, Ren X. Physical metallurgy of Ti–Ni-based shape memory alloys. *Mater Sci* 2005;5:511–678.
- [24] Sakamoto H, Shimizu K. Experimental investigation on cyclic deformation and fatigue behavior of polycrystalline CuAlNi shape memory alloys above Ms. *Trans Japan Inst Metals* 1986;27–8:592–600.
- [25] Van Humbeeck J, Stalmans R. Characteristics of shape memory alloy. In: Otsuka K, Wayman CM, editors. *Shape memory materials*. Cambridge: University Press; 1998. p. 149–83.
- [26] Tadaki T. Cu-based shape memory alloys. In: Otsuka K, Wayman CM, editors. *Shape memory materials*. Cambridge: University Press; 2000. p. 97–116.
- [27] Morin M, Trivero F. Influence of thermal cycling on the reversible martensitic transformation in Cu–Al–Ni shape memory alloy. *Mater Sci Eng A* 1995;196:177–81.
- [28] Silva RJ, Matlakhova LA, Pereira EC, Matlakhov AN, Monteiro SN, Rodríguez RJS. Thermal cycling treatment and structural changes in Cu–Al–Ni monocrystalline alloys. *Mater Sci Forum* V 2006;514–516:692–6.
- [29] Suresh N, Ramamurty U. Effect of aging on mechanical behavior of single crystal Cu–Al–Ni shape memory alloys. *Mater Sci Eng A* 2007;454–455:492–9.
- [30] Pereira EC, Matlakhova LA, Matlakhov AN, Monteiro SN, Carvalho EA. Fracture of a single crystal Cu–Al–Ni alloy. *Braz J Morphol Sci* 2005:349–50.
- [31] Nakata Y, Tadaki T, Shimizu K. Thermal cycling effects in a Cu–Al–Ni shape memory alloy. *Trans Japan Inst Metals* 1985;26–99:646–52.
- [32] Priadko A, Pulnev S, Viahhi I, Vetrov V, Yudin V. Proc of the Institute of Robotics and Technical Cybernetics. Actuators and drives based on Cu–Al–Ni shape memory single crystals. St-Petersburg, Russia; 2000. 21p.
- [33] JCPDS — International Centre for Diffraction Data; 2000. Newton Square, PA, USA, PDF: 11-0010. JCPDS — International Centre for Diffraction Data; 2000. Newton Square, PA, USA, PDF: 07-0108. JCPDS — International Centre for Diffraction Data; 2000. Newton Square, PA, USA, PDF: 28-0016.
- [34] Jouneau PH, Stadelmann P. Electron microscopy image simulation. Lausanne: EPFL; 1998. available from: <http://cecm.insa-lyon.fr/CIOLS/crystal4.pl/>. Centre Interdépartemenal de Microscopie Electronique.
- [35] Wasilewski RJ. The effects of applied stress on the martensitic transformation in TiNi. *Metall Trans* 1971;2:2973–81.
- [36] Wasilewski RJ. Stress-assisted martensite formation in TiNi. *Scr Metall* 1971;5–2:127–30.
- [37] Kovneristyi YK, Fedotov SG, Matlakhova LA. Shape memory and shape reversibility effects in a TiNi alloy as function of deformation. *Phys Metall* 1986;62–2:344–8.
- [38] Kovneristyi YK, Fedotov SG, Matlakhova LA. The Influence of plastic deformation on the structure, shape memory effect and other properties of TiNi alloy. Proc Int Conf on Shape Memory Alloys. Guilin, China, vol. 1; 1986. p. 175–80.